

Magnetic excitations in the geometric frustrated multiferroic CuCrO_2

M. Frontzek^{1,*}, J. T. Haraldsen^{2,3,4}, A. Podlesnyak¹, M. Matsuda¹, A. D. Christianson¹, R. S. Fishman⁴, A. S. Sefat⁴, Y. Qiu^{5,6}, J. R. D. Copley⁵, S. Barilo⁷, S. V. Shiryayev⁷, and G. Ehlers¹

¹*Neutron Scattering Division, Oak Ridge National Laboratory, Oak Ridge, Tennessee 37831, USA*

²*Theoretical Division, Los Alamos National Laboratory, Los Alamos, New Mexico 87545, USA*

³*Center for Integrated Nanotechnologies, Los Alamos National Laboratory, Los Alamos, New Mexico 87545, USA*

⁴*Materials Science and Technology Division, Oak Ridge National Laboratory, Oak Ridge, Tennessee 37831, USA*

⁵*NIST Center for Neutron Research, National Institute of Standards and Technology, Gaithersburg, Maryland 20899, USA*

⁶*Department of Materials Science and Engineering,*

University of Maryland, College Park, Maryland, 20742, USA

⁷*Institute of Solid State and Semiconductor Physics, Minsk 220 072, Belarus*

(Dated: November 2, 2021)

In this paper detailed neutron scattering measurements of the magnetic excitation spectrum of CuCrO_2 in the ordered state below $T_{N1} = 24.2$ K are presented. The spectra are analyzed using a model Hamiltonian which includes intralayer-exchange up to the next-next-nearest neighbor and interlayer-exchange. We obtain a definite parameter set and show that exchange interaction terms beyond the next-nearest neighbor are important to describe the inelastic excitation spectrum. The magnetic ground state structure generated with our parameter set is in agreement with the structure proposed for CuCrO_2 from the results of single crystal diffraction experiments previously published. We argue that the role of the interlayer exchange is crucial to understand the incommensurability of the magnetic structure as well as the spin-charge coupling mechanism.

PACS numbers: 75.25+z, 75.30.Ds, 75.47.Lx, 75.85+t

I. INTRODUCTION

Compounds which exhibit both an ordered magnetic phase and a ferroelectric phase are termed multiferroics. Especially the multiferroics where the electric polarization can be controlled with a magnetic field and vice versa are of continuing interest due to the potential applications. The most promising candidates for such controllable multiferroic have been found among the materials with inherent geometric magnetic frustration.¹

Different mechanisms leading to spin-charge coupling that have been discussed in the literature include the magneto-elastic effect,² the ‘inverse’ Dzyaloshinskii-Moriya interaction,^{3,4} and electric dipole induction through hybridization of $p-d$ orbitals as originally proposed by Arima.⁵ Spin-charge coupling due to magnetostriction can occur in collinear commensurate magnetic structures as for instance observed in RMn_2O_5 , where R is a rare earth metal.² If magnetic order with non-zero chirality exists, which may be commensurate or incommensurate with the lattice, the inverse Dzyaloshinskii-Moriya (DM) interaction induces (by inversion symmetry breaking) an electric polarization component perpendicular to the spiral axis and the propagation vector.³ Systems in which this situation is realized include TbMnO_3 ,^{6–12} MnWO_4 ,^{13–16} $\text{RbFe}(\text{MoO}_4)_2$,^{17,18} LiCu_2O_2 ,^{19–24} and $\text{Ni}_3\text{V}_2\text{O}_8$.^{25–27} Spin-charge coupling through Arima’s mechanism requires a proper-screw magnetic structure where the vector of the polarization is parallel to the screw axis and to the propagation vector, CuFeO_2 is the most prominent example.^{5,28–34}

In this article, we report a detailed analysis of the spin dynamics of the multiferroic system CuCrO_2 which has

already been studied using a variety of techniques such as polarization in applied magnetic and electric fields,^{35,36} electron spin resonance (ESR),³⁷ x-ray emission spectroscopy, (XES)^{38,39} single crystal x-ray diffraction,⁴⁰ neutron diffraction,^{41–45} and inelastic neutron scattering.^{46,47} This system is isostructural to CuFeO_2 and a detailed comparison of the two systems is instructive.

In contrast to CuFeO_2 which becomes multiferroic in an applied magnetic field⁴⁸ or through doping the Fe site with Al,⁴⁹ Ga⁵⁰ or Rh⁵¹, CuCrO_2 enters the multiferroic state in zero field with the magnetic transition. In both compounds the magnetic structure in the multiferroic phase is an incommensurate proper-screw magnetic structure. However, the propagation vector found for CuCrO_2 with $\boldsymbol{\tau} = (\tau, \tau, 0)$ and $\tau = 0.3298(1)$ is very close to the commensurate value. Unlike the propagation vector of CuFeO_2 which in comparison is very different, $\boldsymbol{\tau} = (\tau, \tau, 3/2)$ with $\tau = 0.207$.⁵²

II. EXPERIMENTAL

A detailed account of the sample preparation was given previously.⁴⁵ The trigonal crystal structure (space group $R\bar{3}m$) with lattice parameters $a = 2.97$ Å and $c = 17.110$ Å was confirmed by x-ray powder analysis of crushed crystals. Further characterization with respect to their magnetic properties was done using a SQUID-magnetometer. The obtained susceptibility curves are similar to data published previously.^{36,42,44,53} Identifying the same characteristic points in the susceptibility data as Kimura et al.⁵³ the same two characteristic phase transition temperatures, $T_{N1} = 24.2$ K and $T_{N2} = 23.6$ K, were obtained for our samples. The Curie-

77 Weiss fit between 148 K and 287 K of the inverse suscep-
 78 tibility gave an asymptotic paramagnetic Curie temper-
 79 ature of -200(1) K and an effective moment of 3.88(1) μ_B
 80 per Cr^{3+} ion. Measurements of the magnetization mea-
 81 sured along three orthogonal directions, $[110]$, $[\bar{1}10]$ and
 82 $[001]$, are shown in Fig. 1 below. A phase transition at
 83 $H_{\text{flop}} \sim 5.3$ T can be seen in these data (the value is
 84 determined from the center of gravity of the peak in the
 85 derivative), in agreement with earlier reports.³⁶ At this
 86 phase transition the electrical polarization is flopped³⁶ in
 87 conjunction with a reorientation of the ordered magnetic
 88 moments.⁴⁴

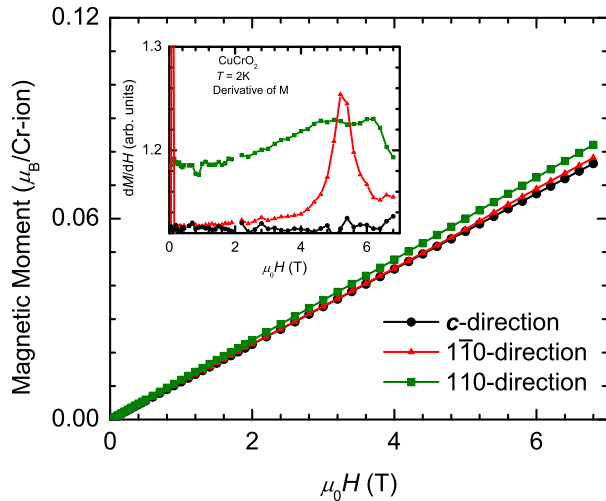


FIG. 1. (Color online) Magnetization measurement along the three main crystallographic directions in CuCrO_2 single crystals at $T = 2$ K. The inset shows the derivative of the magnetization with a peak at H_{flop} in the $[\bar{1}10]$ direction.

89 Ten crystals with a total mass of $m \sim 0.6$ g were co-
 90 aligned on an aluminum sheet covering an area of approx.
 91 20×20 mm for inelastic neutron scattering experiments.
 92 The crystals were platelet like with the c -direction nor-
 93 mal to the plate surface. The horizontal scattering plane
 94 was HLL . Experiments were conducted at the Cold
 95 Neutron Chopper Spectrometer (CNCS) at the Spalla-
 96 tion Neutron Source in Oak Ridge⁵⁴, the HB-1 triple-axis
 97 spectrometer at the High Flux Isotope Reactor in Oak
 98 Ridge, and at the Disk Chopper Spectrometer (DCS) at
 99 the NIST Center for Neutron Research (NCNR).⁵⁵

100 All experiments used a standard orange cryostat in
 101 a temperature range from 1.5 to ~ 100 K. The CNCS
 102 measurements were performed in two settings with dif-
 103 ferent incident neutron energies, 12.1 meV and 3 meV,
 104 respectively. The energy resolution at the elastic line was
 105 0.4350(6) meV full width at half max. (FWHM) at 12.1
 106 meV and 0.0649(1) meV FWHM at 3 meV, respectively.
 107 The HB-1 measurements used constant $k_f = 14.7$ meV
 108 which resulted in an effective energy resolution of 1.84
 109 meV at 7.5 meV. The collimation was 48-60-60-240 with
 110 two additional pyrolytic graphite (PG) filters to suppress
 111 higher order contamination. The DCS measurement was

112 performed with an incident energy of 3.53 meV with a
 113 measured resolution of 0.1 meV (FWHM) at the elastic
 114 line. The data obtained on CNCS and DCS have been
 115 reduced using the DAVE software package.⁵⁶

116 III. THEORY

117 The hexagonal symmetry of the CuCrO_2 lattice pro-
 118 vides a complex network of possible intra- and inter-
 119 layer superexchange pathways⁵⁷ that are described by
 120 the Heisenberg Hamiltonian

$$H = -\frac{1}{2} \sum_{i \neq j} J_{ij} \mathbf{S}_i \cdot \mathbf{S}_j - D_x \sum_i \mathbf{S}_{ix}^2 - D_z \sum_i \mathbf{S}_{iz}^2, \quad (1)$$

121 where \mathbf{S}_i is the local moment on site i . The superex-
 122 change interactions J_{ij} between sites i and j are antifer-
 123 romagnetic when $J_{ij} < 0$. An overview of the exchange
 124 paths in respect to the lattice is given in Fig. 2. The
 125 single-ion anisotropy along the x and z axes is given by
 126 $D_{x,z}$, where $D > 0$ produces easy-axis anisotropy and
 127 $D < 0$ produces easy-plane anisotropy, respectively. The
 128 three-dimensional magnetic state is constructed by stack-
 129 ing the two-dimensional configurations ferromagnetically
 130 along the c -axis.

131 Through an energy minimization of the exchange pa-
 132 rameters and anisotropy, the magnetic ground state con-
 133 figuration is determined through a classical approach de-
 134 scribed in Ref. 58 by defining S_z within any hexagonal
 135 plane as

$$S_z(\mathbf{R}) = A \cdot \sum_{l=0} C_{2l+1} \cos[\tau_x(2l+1)x] \quad (2)$$

136 where the C_{2l+1} harmonics are produced by the easy axis
 137 anisotropy D_z . With C_1 set to 1, the amplitude A is

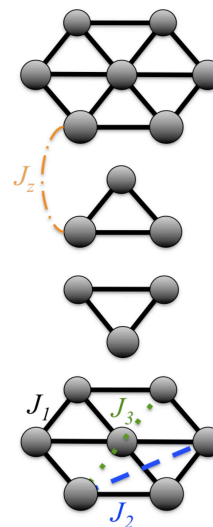


FIG. 2. (Color online) Considered exchange paths in the Heisenberg Hamiltonian.

138 obtained from the condition that the maximum value of
 139 $|S_z(\mathbf{R})|$ equals S . The perpendicular spin components
 140 S_y are given by

$$S_y(\mathbf{R}) = \sqrt{S - S_z(\mathbf{R})^2} \cdot \text{sgn}(\sin(\tau_x x)). \quad (3)$$

141 The ordering wavevector τ_x and coefficients C_{2l+1} are
 142 determined by minimizing the energy on a large unit cell
 143 of size $\sim 10^4 a \times a \times c$, where a is the lattice constant
 144 within a hexagonal plane and c is the separation between
 145 neighboring planes.

146 Based on this magnetic ground state, the spin dynam-
 147 ics are evaluated using a Holstein-Primakoff transforma-
 148 tion, where the spin operators are given by $S_{iz} = S - a_i^\dagger a_i$,
 149 $S_{i+} = \sqrt{2S} a_i$, and $S_{i-} = \sqrt{2S} a_i^\dagger$ (a_i and a_i^\dagger are boson
 150 destruction and creation operators). A rotation of the
 151 local spin operators accounts for the non-collinearity of
 152 the spins.^{59,60}

153 To determine the spin wave (SW) frequencies $\omega_{\mathbf{Q}}$,
 154 we solve the equation-of-motion for the vectors $\mathbf{v}_{\mathbf{Q}} =$
 155 $[a_{\mathbf{Q}}^{(1)}, a_{\mathbf{Q}}^{(1)\dagger}, a_{\mathbf{Q}}^{(2)}, a_{\mathbf{Q}}^{(2)\dagger}, \dots]$, which may be written in terms
 156 of the $2N \times 2N$ matrix $\underline{M}(\mathbf{Q})$ as $id\mathbf{v}_{\mathbf{Q}}/dt = -[\underline{H}_2, \mathbf{v}_{\mathbf{Q}}] =$
 157 $\underline{M}(\mathbf{Q})\mathbf{v}_{\mathbf{Q}}$, where N is the number of spin sites in the unit
 158 cell.⁵⁹ The SW frequencies are then determined from the
 159 condition $\text{Det}[\underline{M}(\mathbf{Q}) - \omega_{\mathbf{Q}}\underline{I}] = 0$. To assure the local sta-
 160 bility of a magnetic phase, all SW frequencies must be
 161 real and positive and all SW weights must be positive.

162 The SW intensities or weights are coefficients of the
 163 spin-spin correlation function:

$$S(\mathbf{Q}, \omega) = \sum_{\alpha\beta} (\delta_{\alpha\beta} - Q_\alpha Q_\beta) S^{\alpha\beta}(\mathbf{Q}, \omega), \quad (4)$$

164 where α and β are x , y , or z .⁶⁰ A more detailed discussion
 165 of this method is contained in Ref. 59. Notice that mag-
 166 netic neutron scattering measurements (INS) only detect
 167 components of the spin fluctuations perpendicular to the
 168 wavevector \mathbf{Q} . The total intensity $I(\mathbf{Q}, \omega)$ for an INS
 169 scan at constant \mathbf{Q} is given by

$$I(\mathbf{Q}, \omega) = S(\mathbf{Q}, \omega) F_{\mathbf{Q}}^2 \exp(-(\omega - \omega_{\mathbf{Q}})^2 / 2\delta^2), \quad (5)$$

170 where δ is the energy resolution and $F_{\mathbf{Q}}$ is the Cr^{3+} mag-
 171 netic form factor.

172 This approach yields additional information on the
 173 magnetic ground state. The magnetic ground state is
 174 not provided for these systems and must therefore be de-
 175 rived from the energy minimization of the Hamiltonian
 176 possible magnetic structures within the $\sim 10^4 a \times a \times c$
 177 cell. Therefore, two energetically degenerate states, for
 178 instance commensurate vs. slightly incommensurate, can
 179 be distinguished.

180 IV. RESULTS

181 The inelastic excitation spectrum of CuCrO_2 in the
 182 HH direction as measured at CNCS with $E_i = 12$ meV

183 is shown in the upper panel of Fig. 3. Integration along
 184 the L direction was in the range $0 < L < 5$ r. l. u.
 185 (relative lattice units) which is justified by a rather small
 186 dispersion along this direction. Integration along the per-
 187 pendicular $H\bar{H}$ direction was within ± 0.025 r. l. u. (cor-
 188 responding to ± 2.5 deg. out of the scattering plane). For
 189 comparison the model calculation is shown in the lower
 190 panel.

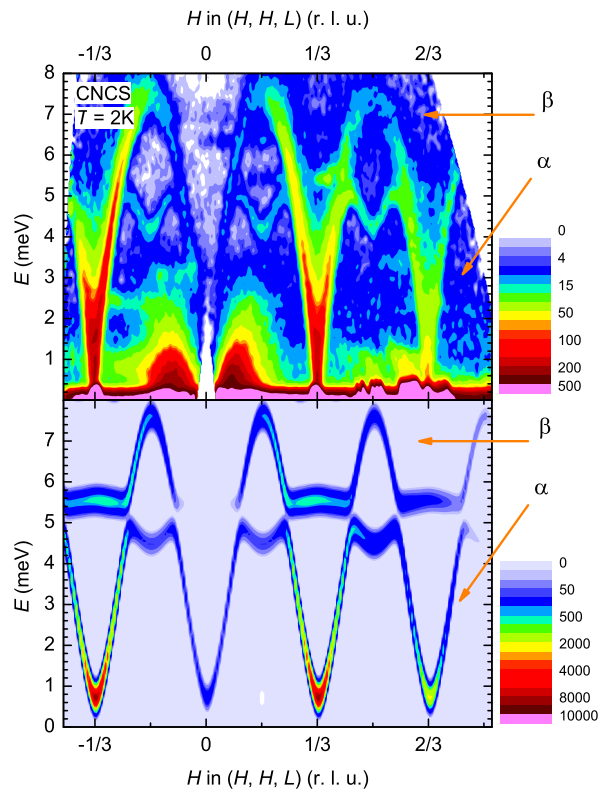


FIG. 3. (Color online) Upper panel: Magnetic excitation spectrum in $S(\mathbf{Q}, \omega)$ of CuCrO_2 measured at $T = 2$ K at CNCS. Integration range along L was from 0 to 5 in r. l. u., and along the $H\bar{H}$ direction ± 0.025 r. l. u.. The intensity around $H = 0$ at low energy originates from the halo of the primary beam. Lower panel: Spin waves computed from the best theoretical model, the modes discussed in the text are marked α , β .

191 The low energy mode α originates from the magnetic
 192 Bragg peak in the vicinity of $H = 1/3$ and flattens off
 193 at around 5 meV. It has a cusp like local energy mini-
 194 mum at the magnetic zone boundary at $H = 1/6$. The
 195 intensity of this mode is strongest in the vicinity of the
 196 Bragg peak and falls off towards the zone boundary. This
 197 mode is mainly influenced by the model parameters J_2 ,
 198 J_3 , D_x and D_z (see above). The minimum of the α mode
 199 at $H = 1/6$ is of considerable interest. It can only be
 200 modeled with the inclusion of an antiferromagnetic next-
 201 next nearest neighbor exchange interaction J_3 . If J_3 is
 202 neglected or ferromagnetic, the excitation would be flat
 203 at $H = 1/6$ or would show a local maximum. Analyz-
 204 ing the intensity of the α mode at the zone boundary,

the measurement shows more intensity at $H = 1/2$ than at $H = 1/6$. In the modeling this leads to a negative in-plane anisotropy constant D_x (otherwise the intensity would be higher at $H = 1/6$). In return, this leads to a ground state with a proper screw magnetic structure rather than a cycloid.

The non-zero anisotropy terms D_x and D_z mean that the α mode must be gapped. The gap is too small to be unambiguously detected at $E_i = 12.1$ meV. However, with improved energy resolution ($E_i = 3$ meV) a gap of ~ 0.5 meV is clearly seen as shown in Fig. 4. Here the integration along the L -direction is only for a small range around $L = 1$. The absolute values of D_x and D_z are adapted in the theoretical calculations to accurately model this gap.

An overall weaker and flat β mode is observed between 5 and 8 meV. The measurement did not resolve whether a crossing of the α and β mode occurs as suggested by the calculation, mainly due to insufficient resolution. The β mode has a maximum of ~ 7.5 meV at the magnetic zone boundaries at $H = 1/6$ and $H = 1/2$. The energy of the β mode at these points is mainly determined by J_2 and to a lesser degree by J_3 . Kajimoto et al.⁴⁶ ascribed the β mode (referred to as “flat component”) to the existence of an interlayer exchange interaction J_z which is inconsistent with our data. In the lower panel of Fig. 3, the computed spin wave excitation spectrum form the best theoretical model is shown. The α and β mode in this energy range determine J_2 and J_3 as well as J_1 to which all parameters are relative. In agreement with data from the literature,^{46,47} a survival of magnetic collective dynamics up to several times T_N is observed at the position of the α mode.

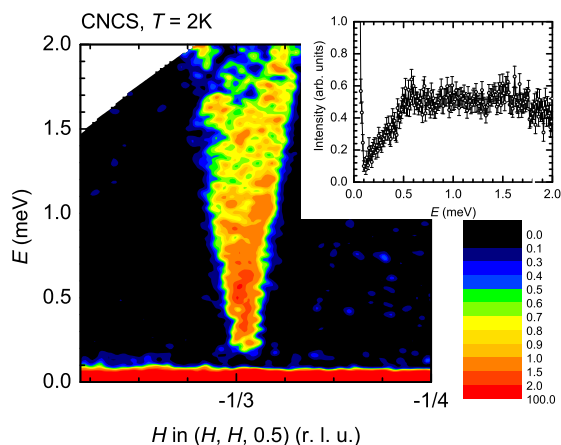


FIG. 4. (Color online) Magnetic excitation spectrum of CuCrO_2 measured at $T = 2$ K at CNCS with 3 meV incident energy. The inset shows a constant- Q cut along the excitation. Error bars represent $\pm 1\sigma$ from counting statistics.

The spin-wave spectrum along the L -direction is dispersion-less for energies above 0.5 meV as already mentioned above. However, below the energy gap of 0.5

meV a modulation can be seen Fig. 5. For an energy transfer of 0.2 meV, the measured intensity along L is higher at the position of the magnetic Bragg peaks compared to the position between. This intensity pattern can

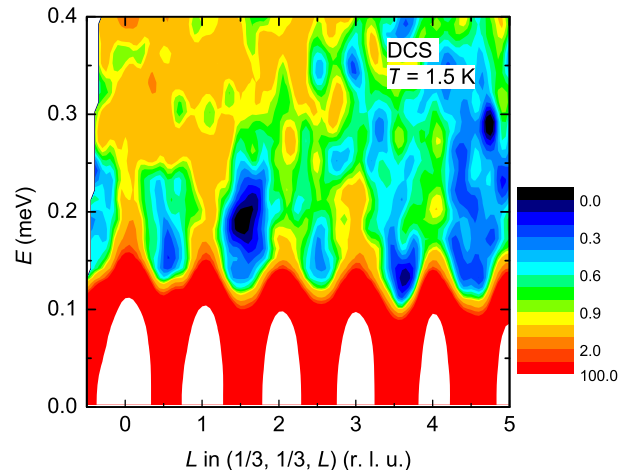


FIG. 5. Magnetic excitation spectrum in $S(Q, \omega)$ of CuCrO_2 measured at $T = 2$ K at DCS with 3.55 meV incident energy. The data is integrated in the HH of 0.32 to 0.34 r. l. u. from the central detector bank. The intensity is color coded in a linear scale with the exception of the elastic Bragg peaks with two orders of magnitude higher intensity.

be reproduced with the introduction of a ferromagnetic interlayer coupling J_z . The magnitude of the interlayer exchange is small as is the effect on the excitation spectrum.

The data presented so far allow the determination of the values for the exchange interaction and the anisotropy terms within the given model. The calculations replicate satisfactorily the α and β excitation modes as shown in the lower panel of 3. The intensity pattern of the DCS measurement (Fig. 5) is modeled with the small interaction term J_z . The interlayer exchange J_z also results in the magnetic ground state with the incommensurate ordering wavevector $\tau_x = 0.329$. Without the interlayer exchange the magnetic ground state would be commensurate. The model Hamiltonian also reproduces the gap in the excitation spectrum, using the anisotropy terms, which as a consequence leads to the splitting of the otherwise degenerated magnetic ground state. This splitting of the degenerate ground state gives rise to another excited state β' at higher energies, with a spin wave dispersion that mirrors the β mode from the ground state but which has an additional gap of 2.2 meV. The intensity of this mode is weaker than the excitations from the ground state and cannot be seen in the CNCS data, likely because, by way of how the (\mathbf{Q}, ω) space is mapped in a time-of-flight measurement with the chosen settings, only $L > 1$ is covered at $\hbar\omega \gtrsim 8$ meV.

Figure 6 shows a contour map of the measurements taken at HB-1. These are constant- E scans with an en-

276 ergy difference of 0.5 meV in the range from 1.5 meV
 277 to 15 meV. The measurements are along the ($HH2$) di-
 278 rection. In this figure, it can be seen that another mode
 279 with nearly the same dispersion exists above the β mode,
 280 which we identify with the β' mode resulting from the
 281 calculations. The coarser energy resolution of HB-1 leads
 282 to a partial blur of the β and β' mode. The calculation
 283 yields a gap between both modes of 2.2 meV at the zone
 284 boundary.

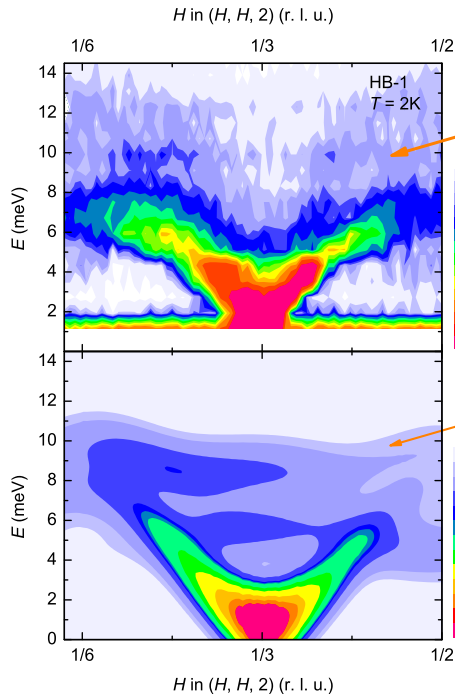


FIG. 6. (Color online) Upper panel: Contour map from constant- E scans of CuCrO_2 measured at $T = 2$ K at HB-1. Lower panel: The corresponding model of the α , β and β' excitations.

285 To summarize the results, the intensity and dispersion
 286 of experimentally observed spin-wave modes in CuCrO_2
 287 have been modeled with a Hamiltonian that includes at
 288 least six free parameters, which are given in Table I.

Set	J_1	J_2	J_3	J_z	D_x	D_z
Ref. 47	-2.3	-0.12	-	-	-0.4*	0.4*
This work	-2.8	-0.48	-0.08	0.02	-0.59	0.48
CuFeO_2	-0.23	-0.12	-0.16	-0.06 [†]	-	0.22

TABLE I. Comparison of the relevant exchange interaction and anisotropy parameters from Ref. 47 (*only one value was fitted) with this work and the results for CuFeO_2 from Ref. 57([†] J_{z1}). Energies are in meV.

289

290

291 Small discrepancies between calculation and measure-
 292 ment suggest the need to include higher order parameters
 293 beyond the ones used here. This is most apparent in the

294 slight discrepancy of the spin-wave velocities. The ve-
 295 locities depend in a non-trivial way from all interactions
 296 and deviations from the model may indicate the need for
 297 magneto-elastic or bi-quadratic terms. While the addition
 298 of J_3 and D_z helps reduce this difference, it is clear
 299 that other interactions may be affecting the system. The
 300 deduction of the parameters in the Hamiltonian has been
 301 based on the approach to incorporate the least necessary
 302 number to describe the excitation spectrum satisfactorily.

303 In comparison to CuFeO_2 , the nearest neighbor in-
 304 tralayer exchange interaction J_1 is one order of magni-
 305 tude stronger in CuCrO_2 , but the interlayer exchange
 306 and the anisotropy parameter D_z are of comparable mag-
 307 nitude.⁶¹ The different magnetic ground states are ex-
 308 plainable with the different ratio of $D/|J_1|$. In CuCrO_2 ,
 309 where this ratio is small, the proper-screw is the stable
 310 magnetic structure, while in CuFeO_2 the four-sublattice
 311 collinear structure is the ground state.⁵⁸ It has been in-
 312 terpreted that the main effect of doping in CuFeO_2 is the
 313 decrease of anisotropy and through this the proper-screw
 314 magnetic structure can be stabilized as ground state in
 315 the doped compounds.⁵⁰ Notably is the difference of the
 316 in-plane anisotropy D_x which is absent in CuFeO_2 where
 317 a Goldstone mode at the incommensurate wavevector is
 318 observed⁵⁷, but present in CuCrO_2 as indicated by the
 319 gap of the α mode. Instead of D_x the observed lattice
 320 distortion in the basal plane is relevant to model the ex-
 321 citation spectra in CuFeO_2 .⁶¹

322 The interlayer exchange in CuFeO_2 leads to a 10-sub
 323 lattice stacking sequence along the c -direction and can be
 324 modeled with one ferromagnetic and two antiferromag-
 325 netic exchange parameters.⁵⁷ The interlayer exchange in
 326 CuCrO_2 seems simpler and can be described with one fer-
 327 romagnetic parameter of similar magnitude. In CuFeO_2
 328 the interlayer exchange has been the most affected pa-
 329 rameter by doping⁶¹ which might explain the difference
 330 between CuCrO_2 and CuFeO_2 .

331 The last marked difference to be discussed is the appar-
 332 ent absence of a structural phase transition in CuCrO_2 .
 333 Strain measurements on CuCrO_2 ⁴⁰ indicate strong mag-
 334 netoelastic coupling, but apparently insufficient to lead
 335 to a phase transition as in CuFeO_2 . In the latter, it
 336 has been demonstrated that the inclusion of bi-quadratic
 337 terms in the Hamiltonian are relevant in the prediction of
 338 the phase diagram.⁶² In CuCrO_2 , the bi-quadratic terms
 339 seem less relevant for the understanding of the magnetic
 340 ground state but probably cause the slight discrepancy of
 341 the spin-wave velocities between model and experiment.

342

V. CONCLUSION

343

344 A detailed investigation of the magnetic excitation
 345 spectrum of CuCrO_2 , at low temperatures has been per-
 346 formed using neutron scattering techniques. The exci-
 347 tation spectrum has been used to deduce the relevant
 348 exchange interaction and anisotropy parameters. The
 parameter set points to a ground state with an incom-

349 mensurate proper-screw magnetic structure in agreement
 350 with results published earlier.^{42,45,47} Antiferromagnetic
 351 intralayer exchange has to be considered up to next-next
 352 nearest neighbor in order to be consistent with the ex-
 353 perimental data.

354 We have also shown that interlayer exchange is relevant
 355 for CuCrO_2 which can thus no longer be considered as
 356 a quasi two-dimensional system. The multiferroic prop-
 357 erties of CuCrO_2 have been explained within the light
 358 of the Arima model which does not consider order be-
 359 tween the spiral planes. It is an interesting question in
 360 which way the interlayer exchange interaction in CuCrO_2
 361 affects its multiferroic properties.

ACKNOWLEDGMENTS

363 We acknowledge the technical and scientific support
 364 from the staff at SNS, HFIR, and NIST. This research
 365 was sponsored by the Division of Materials Sciences and
 366 Engineering of the U. S. Department of Energy. This
 367 work utilized facilities supported in part by the Na-
 368 tional Science Foundation under Agreement No. DMR-
 369 0944772. Research at Oak Ridge National Laboratory's
 370 Spallation Neutron Source was supported by the Scien-
 371 tific User Facilities Division, Office of Basic Energy Sci-
 372 ences, U. S. Department of Energy. Some theoretical
 373 aspects of this work has been supported by the Center
 374 for Integrated Nanotechnologies, a U.S. Department of
 375 Energy, Office of Basic Energy Sciences user facility. Los
 376 Alamos National Laboratory is operated by Los Alamos
 377 National Security, LLC, for the National Nuclear Security
 378 Administration of the U.S. Department of Energy under
 379 contract DE-AC52-06NA25396. The work in Minsk was
 380 supported in part by Belarusian Fund for Basic Scientific
 381 Research, grant No F10R-154.

382 * Corresponding author: frontzekmd@ornl.gov

383 ¹ S.-W. Cheong and M. Mostovoy, *Nature Materials*, **6**, 13
 384 (2007).

385 ² L. C. Chapon, P. G. Radaelli, G. R. Blake, S. Park, and
 386 S.-W. Cheong, *Phys. Rev. Lett.*, **96**, 097601 (2006).

387 ³ H. Katsura, N. Nagaosa, and A. V. Balatsky, *Phys. Rev.*
 388 *Lett.*, **95**, 057205 (2005).

389 ⁴ M. Mochizuki and N. Furukawa, *Phys. Rev. Lett.*, **105**,
 390 187601 (2010).

391 ⁵ T. Arima, *Journal of the Physical Society of Japan*, **76**,
 392 073702 (2007).

393 ⁶ M. Kenzelmann, A. B. Harris, S. Jonas, C. Broholm,
 394 J. Schefer, S. B. Kim, C. L. Zhang, S.-W. Cheong, O. P.
 395 Vajk, and J. W. Lynn, *Phys. Rev. Lett.*, **95**, 087206
 396 (2005).

397 ⁷ Y. Takahashi, N. Kida, Y. Yamasaki, J. Fujioka, T. Arima,
 398 R. Shimano, S. Miyahara, M. Mochizuki, N. Furukawa,
 399 and Y. Tokura, *Phys. Rev. Lett.*, **101**, 187201 (2008).

400 ⁸ S. B. Wilkins, T. R. Forrest, T. A. W. Beale, S. R. Bland,
 401 H. C. Walker, D. Mannix, F. Yakhou, D. Prabhakaran,
 402 A. T. Boothroyd, J. P. Hill, P. D. Hatton, and D. F.
 403 McMorrow, *Phys. Rev. Lett.*, **103**, 207602 (2009).

404 ⁹ N. Aliouane, K. Schmalzl, D. Senff, A. Maljuk, K. Prokes,
 405 M. Braden, and D. N. Argyriou, *Phys. Rev. Lett.*, **102**,
 406 207205 (2009).

407 ¹⁰ R. Kajimoto, H. Sagayama, K. Sasai, T. Fukuda, S. Tsut-
 408 sui, T. Arima, K. Hirota, Y. Mitsui, H. Yoshizawa, A. Q. R.
 409 Baron, Y. Yamasaki, and Y. Tokura, *Phys. Rev. Lett.*,
 410 **102**, 247602 (2009).

411 ¹¹ F. Fabrizi, H. C. Walker, L. Paolasini, F. de Bergevin,
 412 A. T. Boothroyd, D. Prabhakaran, and D. F. McMorrow,
 413 *Phys. Rev. Lett.*, **102**, 237205 (2009).

414 ¹² A. M. Shuvaev, V. D. Travkin, V. Y. Ivanov, A. A. Mukhin,
 415 and A. Pimenov, *Phys. Rev. Lett.*, **104**, 097202 (2010).

416 ¹³ G. Lautenschläger, H. Weitzel, T. Vogt, R. Hock, A. Böhm,
 417 M. Bonnet, and H. Fuess, *Phys. Rev. B*, **48**, 6087 (1993).

418 ¹⁴ K. Taniguchi, N. Abe, H. Umetsu, H. A. Katori, and
 419 T. Arima, *Phys. Rev. Lett.*, **101**, 207205 (2008).

420 ¹⁵ K. Taniguchi, N. Abe, S. Ohtani, and T. Arima, *Phys.*
 421 *Rev. Lett.*, **102**, 147201 (2009).

422 ¹⁶ K. V. Shanavas, D. Choudhury, I. Dasgupta, S. M. Sharma,
 423 and D. D. Sarma, *Phys. Rev. B*, **81**, 212406 (2010).

424 ¹⁷ S. A. Klimin, M. N. Popova, B. N. Mavrin, P. H. M. van
 425 Loosdrecht, L. E. Svistov, A. I. Smirnov, L. A. Prozorova,
 426 H.-A. K. von Nidda, Z. Seidov, A. Loidl, A. Y. Shapiro,
 427 and L. N. Demianets, *Phys. Rev. B*, **68**, 174408 (2003).

428 ¹⁸ M. Kenzelmann, G. Lawes, A. B. Harris, G. Gasparovic,
 429 C. Broholm, A. P. Ramirez, G. A. Jorge, M. Jaime,
 430 S. Park, Q. Huang, A. Y. Shapiro, and L. A. Demianets,
 431 *Phys. Rev. Lett.*, **98**, 267205 (2007).

432 ¹⁹ T. Masuda, A. Zheludev, A. Bush, M. Markina, and
 433 A. Vasiliev, *Phys. Rev. Lett.*, **92**, 177201 (2004).

434 ²⁰ T. Masuda, A. Zheludev, B. Roessli, A. Bush, M. Markina,
 435 and A. Vasiliev, *Phys. Rev. B*, **72**, 014405 (2005).

436 ²¹ H. J. Xiang and M.-H. Whangbo, *Phys. Rev. Lett.*, **99**,
 437 257203 (2007).

438 ²² S. W. Huang, D. J. Huang, J. Okamoto, C. Y. Mou, W. B.
 439 Wu, K. W. Yeh, C. L. Chen, M. K. Wu, H. C. Hsu, F. C.
 440 Chou, and C. T. Chen, *Phys. Rev. Lett.*, **101**, 077205
 441 (2008).

442 ²³ D. Hübner, U. Nagel, T. Rõõm, Y. J. Choi, C. L. Zhang,
 443 S. Park, and S.-W. Cheong, *Phys. Rev. B*, **80**, 100402(R)
 444 (2009).

445 ²⁴ S. Seki, Y. Yamasaki, M. Soda, M. Matsuura, K. Hirota,
 446 and Y. Tokura, *Phys. Rev. Lett.*, **100**, 127201 (2008).

447 ²⁵ G. Lawes, M. Kenzelmann, N. Rogado, K. H. Kim, G. A.
 448 Jorge, R. J. Cava, A. Aharony, O. Entin-Wohlman, A. B.
 449 Harris, T. Yildirim, Q. Z. Huang, S. Park, C. Broholm,
 450 and A. P. Ramirez, *Phys. Rev. Lett.*, **93**, 247201 (2004).

451 ²⁶ G. Lawes, A. B. Harris, T. Kimura, N. Rogado, R. J. Cava,
 452 A. Aharony, O. Entin-Wohlman, T. Yildirim, M. Kenzel-
 453 mann, C. Broholm, and A. P. Ramirez, *Phys. Rev. Lett.*,

- 454 **95**, 087205 (2005).
- 455 ²⁷ A. B. Harris, T. Yildirim, A. Aharony, and O. Entin-
456 Wohlman, Phys. Rev. B, **73**, 184433 (2006).
- 457 ²⁸ M. Uhrmacher, R. N. Attili, K. P. Lieb, K. Winzer, and
458 M. Mekata, Phys. Rev. Lett., **76**, 4829 (1996).
- 459 ²⁹ F. Ye, J. A. Fernandez-Baca, R. S. Fishman, Y. Ren, H. J.
460 Kang, Y. Qiu, and T. Kimura, Phys. Rev. Lett., **99**,
461 157201 (2007).
- 462 ³⁰ F. Wang and A. Vishwanath, Phys. Rev. Lett., **100**, 077201
463 (2008).
- 464 ³¹ J. T. Haraldsen, M. Swanson, G. Alvarez, and R. S. Fish-
465 man, Phys. Rev. Lett., **102**, 237204 (2009).
- 466 ³² T. Nakajima, S. Mitsuda, K. Takahashi, M. Ya-
467 mano, K. Masuda, H. Yamazaki, K. Prokes, K. Kiefer,
468 S. Gerischer, N. Terada, H. Kitazawa, M. Matsuda,
469 K. Kakurai, H. Kimura, Y. Noda, M. Soda, M. Matsuura,
470 and K. Hirota, Phys. Rev. B, **79**, 214423 (2009).
- 471 ³³ G. Quirion, M. L. Plumer, O. A. Petrenko, G. Balakrish-
472 nan, and C. Proust, Phys. Rev. B, **80**, 064420 (2009).
- 473 ³⁴ T. T. A. Lummen, C. Strohm, H. Rakoto, and P. H. M.
474 van Loosdrecht, Phys. Rev. B, **81**, 224420 (2010).
- 475 ³⁵ S. Seki, Y. Onose, and Y. Tokura, Phys. Rev. Lett., **101**,
476 067204 (2008).
- 477 ³⁶ K. Kimura, H. Nakamura, S. Kimura, M. Hagiwara, and
478 T. Kimura, Phys. Rev. Lett., **103**, 107201 (2009).
- 479 ³⁷ H. Yamaguchi, S. Ohtomo, S. Kimura, M. Hagiwara,
480 K. Kimura, T. Kimura, T. Okuda, and K. Kindo, Phys.
481 Rev. B, **81**, 033104 (2010).
- 482 ³⁸ T. Arnold, D. J. Payne, A. Bourlange, J. P. Hu, R. G.
483 Egdell, L. F. J. Piper, L. Colakerol, A. DeMasi, P.-A.
484 Glans, T. Learmonth, K. E. Smith, J. Guo, D. O. Scanlon,
485 A. Walsh, B. J. Morgan, and G. W. Watson, Phys. Rev.
486 B, **79**, 075102 (2009).
- 487 ³⁹ D. Shin, J. S. Foord, D. J. Payne, T. Arnold, D. J. Aston,
488 R. G. Egdell, K. G. Godinho, D. O. Scanlon, B. J. Morgan,
489 G. W. Watson, E. Mugnier, C. Yaicle, A. Rougier, L. Co-
490 lakerol, P. A. Glans, L. F. J. Piper, and K. E. Smith,
491 Phys. Rev. B, **80**, 233105 (2009).
- 492 ⁴⁰ K. Kimura, T. Otani, H. Nakamura, Y. Wakabayashi, and
493 T. Kimura, Journal of the Physical Society of Japan, **78**,
494 113710 (2009).
- 495 ⁴¹ H. Kadowaki, H. Kikuchi, and Y. Ajiro,
496 Journal of Physics: Condensed Matter, **2**, 4485 (1990).
- 497 ⁴² M. Poienar, F. Damay, C. Martin, V. Hardy, A. Maignan,
498 and G. André, Phys. Rev. B, **79**, 014412 (2009).
- 499 ⁴³ M. Soda, K. Kimura, T. Kimura, M. Matsuura, and K. Hi-
500 rota, Journal of the Physical Society of Japan, **78**, 124703
501 (2009).
- 502 ⁴⁴ M. Soda, K. Kimura, T. Kimura, and K. Hirota, Phys.
503 Rev. B, **81**, 100406(R) (2010).
- 504 ⁴⁵ M. Frontzek, G. Ehlers, A. Podlesnyak, H. Cao, M. Mat-
505 suda, O. Zaharko, N. Aliouane, S. Barilo, and S. Shiryaev,
506 Phys. Rev. B (2011, submitted).
- 507 ⁴⁶ R. Kajimoto, K. Nakajima, S. Ohira-Kawamura, Y. Ina-
508 mura, K. Kakurai, M. Arai, T. Hokazono, S. Oozono, and
509 T. Okuda, Journal of the Physical Society of Japan, **79**,
510 123705 (2010).
- 511 ⁴⁷ M. Poienar, F. Damay, C. Martin, J. Robert, and S. Petit,
512 Phys. Rev. B, **81**, 104411 (2010).
- 513 ⁴⁸ T. Kimura, J. C. Lashley, and A. P. Ramirez, Phys. Rev.
514 B, **73**, 220401(R) (2006).
- 515 ⁴⁹ S. Seki, Y. Yamasaki, Y. Shiomi, S. Iguchi, Y. Onose, and
516 Y. Tokura, Phys. Rev. B, **75**, 100403(R) (2007).
- 517 ⁵⁰ J. T. Haraldsen and R. S. Fishman, Phys. Rev. B, **82**,
518 144441 (2010).
- 519 ⁵¹ B. Kundys, A. Maignan, D. Pelloquin, and C. Simon, Solid
520 State Sciences, **11**, 1035 (2009), ISSN 1293-2558, e-MRS
521 symposium N and R.
- 522 ⁵² T. Nakajima, S. Mitsuda, S. Kanetsuki, K. Prokes,
523 A. Podlesnyak, H. Kimura, and Y. Noda, Journal of the
524 Physical Society of Japan, **76**, 043709 (2007).
- 525 ⁵³ K. Kimura, H. Nakamura, K. Ohgushi, and T. Kimura,
526 Phys. Rev. B, **78**, 140401(R) (2008).
- 527 ⁵⁴ T. E. Mason, D. Abernathy, I. Anderson, J. Ankner,
528 T. Egami, G. Ehlers, A. Ekkebus, G. Granroth, M. Hagen,
529 K. Herwig, J. Hodges, C. Hoffmann, C. Horak, L. Horton,
530 F. Klose, J. Larese, A. Mesezar, D. Myles, J. Neuefeind,
531 M. Ohl, C. Tulk, X. L. Wang, and J. Zhao, Physica B,
532 **385-386**, 955 (2006).
- 533 ⁵⁵ J. R. D. Copley and J. C. Cook, Chem. Phys., **292**, 447
534 (2003).
- 535 ⁵⁶ R. T. Azuah, L. R. Kneller, Y. Qiu, P. L. W. Tregenna-
536 Piggott, C. M. Brown, J. R. D. Copley, and R. M. Dimeo,
537 J. Res. Natl. Inst. Stan. Technol., **114**, 341 (209).
- 538 ⁵⁷ R. S. Fishman, F. Ye, J. A. Fernandez-Baca, J. T. Harald-
539 sen, and T. Kimura, Phys. Rev. B, **78**, 140407(R) (2008).
- 540 ⁵⁸ R. S. Fishman and S. Okamoto, Phys. Rev. B, **81**,
541 020402(R) (2010).
- 542 ⁵⁹ J. T. Haraldsen and R. S. Fishman, J. Phys.: Condens.
543 Matter, **21**, 216001 (2009).
- 544 ⁶⁰ M. E. Zhitomirsky and I. A. Zaliznyak, Phys. Rev. B, **53**,
545 3428 (1996).
- 546 ⁶¹ J. T. Haraldsen, F. Ye, R. S. Fishman, J. A. Fernandez-
547 Baca, Y. Yamaguchi, K. Kimura, and T. Kimura, Phys.
548 Rev. B, **82**, 020404(R) (2010).
- 549 ⁶² M. L. Plumer, Phys. Rev. B, **76**, 144411 (2007).